A method for high-energy, low-dose mammography using edge illumination x-ray phase-contrast imaging

2016 Phys. Med. Biol. 61 8750

(http://iopscience.iop.org/0031-9155/61/24/8750)

OPEN ACCESS
IOP Publishing | Institute of Physics and Engineering in Medicine Physics in Medicine & Biology
Phys. Med. Biol. **61** (2016) 8750–8761 doi:10.1088/1361-6560/61/24/8750

A method for high-energy, low-dose mammography using edge illumination x-ray phase-contrast imaging

Paul C Diemoz[1], Alberto Bravin[2], Anikó Sztrókay-Gaul[3], Marie Ruat[2], Susanne Grandl[3], Doris Mayr[4], Sigrid Auweter[3], Alberto Mittone[2,5], Emmanuel Brun[2,5], Cyril Ponchut[2], Maximilian F Reiser[3], Paola Coan[3,5] and Alessandro Olivo[1]

[1] Department of Medical Physics and Biomedical Engineering, University College London, London, WC1E 6BT, UK
[2] European Synchrotron Radiation Facility, 38043 Grenoble, France
[3] Institute for Clinical Radiology, Ludwig-Maximilians University, 81377 Munich, Germany
[4] Institute for Pathology, Ludwig-Maximilians University, 80337 Munich, Germany
[5] Department of Physics, Ludwig-Maximilians University, 85748 Garching, Germany

E-mail: Paola.Coan@physik.uni-muenchen.de

Received 16 May 2016, revised 6 October 2016
Accepted for publication 26 October 2016
Published 28 November 2016

Abstract

Since the breast is one of the most radiosensitive organs, mammography is arguably the area where lowering radiation dose is of the uttermost importance. Phase-based x-ray imaging methods can provide opportunities in this sense, since they do not require x-rays to be stopped in tissue for image contrast to be generated. Therefore, x-ray energy can be considerably increased compared to those usually exploited by conventional mammography. In this article we show how a novel, optimized approach can lead to considerable dose reductions. This was achieved by matching the edge-illumination phase method, which reaches very high angular sensitivity also at high x-ray energies, to an appropriate image processing algorithm and to a virtually noise-free detection technology capable of reaching almost 100% efficiency at the same energies. Importantly, while proof-of-concept was obtained at a synchrotron, the method has potential for a translation to conventional sources.

Keywords: mammography, x-ray phase-contrast imaging, phase retrieval, dose reduction

(Some figures may appear in colour only in the online journal)

Introduction

X-ray phase contrast imaging (XPCI) generates contrast based on refraction and interference, rather than attenuation (Davis *et al* 1995, Snigirev *et al* 1995, Olivo *et al* 2001, 2007a, Pfeiffer *et al* 2006, Wilkins *et al* 2014). This has two significant implications for diagnostic radiology and other applications of x-ray imaging. First, features classically considered x-ray invisible can be detected, and the visibility of all image details enhanced (Bravin *et al* 2013). Secondly, since generation of image contrast does not require x-rays to be absorbed in the sample, images can be acquired at much higher energies than in conventional radiology, thus potentially achieving significant reductions in radiation dose. This would be extremely important in several clinical applications and especially for the breast, which is one of the most radiosensitive organs (ICRP 2007).

So far, most research has focused on the contrast improvement aspect, since enhanced visibility can lead to earlier detection of important diseases. Various areas of application have been investigated, among which mammography is arguably the most advanced, and indeed the only one where clinical experimentation is currently pursued, albeit with synchrotron radiation (Castelli *et al* 2011). Meanwhile, approaches have emerged that allow implementing XPCI with conventional x-ray sources (Pfeiffer *et al* 2006, Olivo *et al* 2007a), thus potentially enabling its clinical transfer.

This Article focuses on the dose reduction aspect, which has so far proven problematic. At best, previous XPCI studies on breast imaging showed radiation doses compatible with clinical requirements (Keyriläinen *et al* 2008, Castelli *et al* 2011, Zhao *et al* 2012, Olivo *et al* 2013), while most others significantly exceeded clinical limits (Stampanoni *et al* 2011, Grandl *et al* 2013, Sztrokay *et al* 2013). Especially outside synchrotrons, doses that exceed clinical limits by one and several orders of magnitude in planar (Stampanoni *et al* 2011) and CT (Grandl *et al* 2013) implementations, respectively, are typically reported.

In this work, we propose to exploit an approach based on the edge illumination (EI) XPCI technique, which has been under continuous development at University College London in recent years (Olivo *et al* 2001, 2007a, 2013). Not only was this technique shown to provide high angular sensitivity (Diemoz *et al* 2013a, 2013b), but also to enable low-dose implementations (Hagen *et al* 2014). The main reason for this is that the main optical element is placed before the sample, thus protecting it from unwanted dose delivery. While in some implementations there is a second element placed in contact with the detector, this is built on a low-absorbing graphite substrate (Munro *et al* 2012), thus not limiting the dose efficiency of the technique. Here we show how an appropriate translation of this concept to higher x-ray energies, together with an innovative retrieval algorithm, can lead to significant dose reductions in mammography. Importantly, in previous work it was demonstrated that the EI-XPCI technique is compatible with the use of commercial x-ray tubes (Olivo *et al* 2007a, Ignatyev *et al* 2011, Munro *et al* 2012), while still achieving high sensitivity to phase signals (Diemoz *et al* 2013b), and thus the results presented here may be potentially translated in the future to clinical applications.

Materials and methods

Phase-contrast imaging setup

Initial validation was obtained at the ID17 biomedical beamline of the European Synchrotron Radiation Facility (ESRF, Grenoble, France). The EI setup is schematised in figure 1(a): it consists of two slits, one immediately before the sample and one in contact with the detector, slightly misaligned with respect to each other. Image contrast is generated by sample-induced

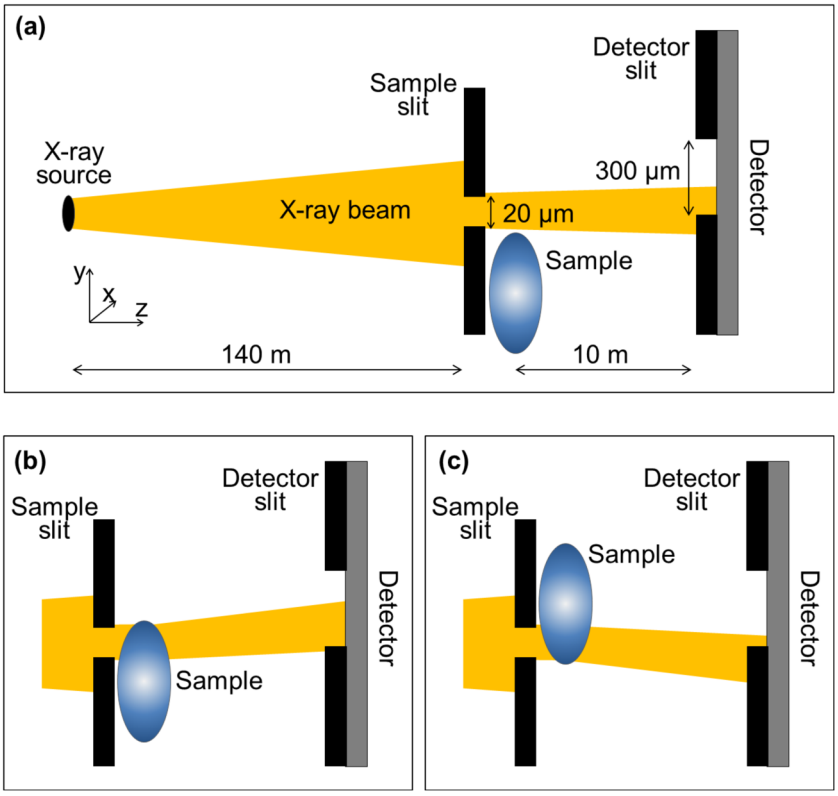

Figure 1. Schematic diagram of the EI experimental setup employed at the ESRF (not to scale). (a) Case with the sample out of the beam. (b) Case with the sample refracting x-rays upwards. (c) Case with the sample refracting x-rays downwards. The beam is shaped to a 20 μm vertical dimension by means of a tungsten carbide slit placed immediately before the sample. This was fabricated to the author's design by UNT (Morbier, France). A slit with a larger (300 μm) vertical aperture is placed in front of the detector, at a distance of 10 m from the sample. This aperture is kept larger in order to collect all x-rays refracted by the sample, thus maximizing the signal. The apertures in the two slits are vertically mismatched such that, in the absence of the sample, about 50% of the beam created by the pre-sample slit enters the aperture in the detector slit, while the remaining 50% falls just outside it and is therefore absorbed. Any refraction caused by a sample introduced downstream of the pre-sample slit would change this fraction, thus creating detectable contrast (see (b) and (c)).

refraction (the refraction angle being proportional to the spatial derivative of the x-ray phase shift). This causes x-rays to be deviated from the absorbing part of the slit into the slit aperture, thus increasing the detected intensity (figure 1(b)), or vice-versa, leading to decreased intensity (figure 1(c)). In this implementation, only one detector line at a time is illuminated, and a vertical scan of the sample through the beam is required to produce a 2D image; this is avoided if a mask with multiple apertures is used rather than a single slit (Olivo *et al* 2007a, 2013, Ignatyev *et al* 2011). This will be pursued in future studies and was not considered necessary for this proof-of-concept work. In addition to XPCI images, corresponding attenuation images were also acquired with the same setup for comparison purposes. In this case, the slit

in front of the detector was removed, the samples were placed in contact with the detector, and the full sample-detector assembly was scanned vertically through the beam. For both XPCI and absorption acquisitions, a continuous vertical scan of speed 0.5 mm s^{-1} was employed, and frames were acquired every 40 ms (which includes 35 ms integration time and 5 ms readout time), leading to an effective scanning step of 20 μm.

Energy optimization

The energy optimization aspect had to be considered. While dose initially decreases for x-ray energies above those used in conventional mammography, the process does not continue indefinitely. Indeed, the energy absorption coefficient of the breast tissue has a minimum at around 80 keV, due to the increase in the Compton cross-section at high energies (Mittone *et al* 2014). Moreover, the refraction angle decreases as well, being inversely proportional to the square of the energy. This shifts the optimum energy towards lower values. While precise optimization is feature-specific thus requiring Monte-Carlo approaches, an approximated estimate of 60 keV was considered sufficient for the purposes of this proof-of-concept study.

Detector technology

Another aspect that needed to be addressed is the decreased efficiency of x-ray detectors at increased energies. Novel technology based on the hybridization of thick CdTe/CZT crystals to single photon counting readout chips has recently emerged that can overcome this (Ruat *et al* 2012). We have used the MAXIPIX-CdTe detector developed at the ESRF: it features a 1 mm thick single crystal CdTe sensor hybridized to 4 Timepix chips, arranged in an array of 512 $\times$ 512 pixels at 55 μm pitch (Ponchut *et al* 2011). As well as achieving an almost 100% detection efficiency at energies up to 60 keV, it minimizes image noise through its energy thresholding feature. This minimization of noise to (inescapable) Poisson fluctuations, alongside the high angular sensitivity of EI-XPCI (Diemoz *et al* 2013a), led to maximization of contrast-to-noise ratio in the images.

Image processing of phase-contrast images

This study also exploits a novel approach to data processing, developed in Diemoz *et al* (2015). If x-ray energy is increased, absorption contrast tends to disappear, and images bear little resemblance with conventional ones. In particular, since most current XPCI methods are 'differential', phase contrast only arises at the interfaces between tissue types (i.e. there is no 'area' contrast, see figure 2(c)). This can be overcome through a recently developed phase-retrieval algorithm (Diemoz *et al* 2015), which transforms a 'differential' phase image into an 'enhanced' version of the conventional image radiologists are familiar with. Most importantly, it is a 'single-shot' retrieval method, which represents a significant simplification of the acquisition procedure, as well as an essential aspect when dose reductions are pursued.

In particular, if the refraction angles are small, the normalized signal in a raw EI image can be expressed as Diemoz *et al* (2013a, 2015):

$$S(x,y) = T(x,y)\,[C(y_e) - C'(y_e)k^{-1}z\,\nabla_y\,\phi - C(y_e)k^{-1}z\,\nabla_x\,(T\,\nabla_x\,\phi)] \qquad (1)$$

where C is the illumination curve obtained by vertically scanning the detector slit and C' its derivative (Diemoz *et al* 2013a), y_e is the position of the slit, z is the distance between sample and detector, and k is the wave number; x and y are the spatial coordinates in the plane of the sample, the first being parallel to the slit aperture, while the latter orthogonal to it. T and ϕ are the transmission through the object and the phase shift, respectively. Note that the Compton scattered photons are effectively removed from the transmitted beam due to the large propagation distance and the presence of the detector mask, thus eliminating potential image blurring due to scattering, an effect similar to that obtained with the anti-scatter grids employed in conventional mammographic systems.

The retrieval algorithm assumes that the sample material is approximately homogeneous, such that the ratio $\gamma = \delta/\mu$ is constant across the field of view, with δ being the refractive index and μ the linear attenuation coefficient. Under this assumption, the two quantities T and ϕ depend on a single unknown parameter, the projected electron density map $\rho_{e,p}$ of the sample. In fact, they can be expressed as $T = \exp(-2\pi\gamma^{-1}k^{-2}r_0\rho_{e,p})$ and $\phi = 2\pi k^{-1}r_0\rho_{e,p}$ respectively (Diemoz *et al* 2015), where r_0 is the classical electron radius. It was demonstrated that equation (1) can be inverted to retrieve the object phase map from a single EI image, through the following equation (Diemoz *et al* 2015):

$$\phi = k\gamma \log\left[F^{-1}\left\{\frac{F\{S\}}{1 + \mathrm{i}2\pi\gamma z C'(y_e)C(y_e)^{-1}\nu_y + 4\pi\gamma z\nu_x^2}\right\}\right] \tag{2}$$

where F and F^{-1} indicate forward and inverse Fourier transform, and $\nu_{x,y}$ are the Fourier space coordinates along the two directions x and y in the plane of the object. Equation (2) can be implemented efficiently by making use of the fast Fourier transform. This algorithm was shown to be highly stable against noise in the experimental images (Diemoz *et al* 2016), thus potentially enabling further dose reductions.

It can be seen that the assumption of a quasi-homogeneous object is quite accurately verified in the breast. By considering the elemental compositions of adipose and glandular tissues (Hammerstein *et al* 1979), and the μ and δ values of the single elements (Henke *et al* 1993), in fact, the following values are obtained at 60 keV: $\delta_{ad} = 5.95 \cdot 10^{-8}$, $\delta_{gl} = 6.60 \cdot 10^{-8}$, $\mu_{ad} = 0.1852\,\mathrm{cm}^{-1}$ and $\mu_{gl} = 0.2132\,\mathrm{cm}^{-1}$. These give $\gamma = 3.21 \cdot 10^{-7}\,\mathrm{cm}$ for adipose tissue and $\gamma = 3.10 \cdot 10^{-7}\,\mathrm{cm}$ for glandular tissue, which differ by only 3.7%.

Reference images

Conventional images of *ex vivo* breast samples were acquired using a standard mammography unit (Selenia Dimensions by Hologic) operated manually at 32 kV and 221 mAs. The detector is an amorphous selenium TFT-based direct conversion system, with a pixel size of 70 μm.

Dosimetry

The radiation entrance doses (air kerma) delivered with the phase-contrast setup were measured by scanning a PTW Semiflex ionization chamber through the collimated beam (at the same speed used for the samples during image acquisition). The chamber, which has a sensitive volume of 0.125 cm^3 and is operated at 400 V (according to PTW recommendations), is read-out by a PTW Webline electrometer (PTW, Freiburg, Germany). It was calibrated using a

^{60}Co radiation source; based on the manufacturer manual, the nominal useful energy range is 30 keV–50 MeV and the energy response within this rage differs by 4% at most.

The mean glandular dose (MGD) values have then been calculated using the following formula:

$$\mathrm{MGD} = k_{\mathrm{D}} \cdot k_{\mathrm{MGD}} \cdot D_{\mathrm{in}} \tag{3}$$

where k_{D} is the conversion factor from kerma (dose in air) D_{in} to average dose to the sample, and k_{MGD} is the conversion factor from average dose to MGD. The first coefficient was estimated through Monte Carlo simulations using GATE (Mittone *et al* 2013), with the PENELOPE physics models considering the three following fundamental interactions: Compton scattering, Rayleigh scattering and photoelectric effect. The method used to calculate this coefficient was the one proposed by Boone (1999): the sample was modelled as a homogeneous parallelepiped, and a 50% fraction of glandular tissue was assumed, with the breast chemical composition following the one proposed by Hammerstein *et al* (1979). The obtained values are $k_{\mathrm{D}} = 0.91 \pm 0.01$ and $k_{\mathrm{D}} = 0.88 \pm 0.02$, respectively for a breast sample thickness of 2 cm and 4 cm. The second coefficient was estimated using the analytical method presented in Mittone *et al* (2014), and is equal to 1.10 for both samples.

The MGD values for the hospital measurements have been calculated using the protocol described in DIN Report (2013). In particular, the MGD is found through the formula:

$$\mathrm{MGD} = g \cdot c \cdot s \cdot D_{\mathrm{in}} \tag{4}$$

where the measured entrance dose is multiplied by the tabulated factors g, c, and s, taking into account respectively the beam quality, the breast tissue thickness and composition and the anode-filter combination.

Sample preparation

Within 1 h after ablation, the ablated breast tissues were fixed in a 4% formaldehyde solution. Clinical standard histopathological workup was completed before data acquisition: the formaldehyde-fixed tissues were cut into 5 mm thick slices, and macroscopically suspicious and representative tissue sections (max. $3.0 \times 2.0 \times 0.5\,\mathrm{cm}^3$) were resected for standard paraffin embedding and automatic staining. For imaging purposes, the samples were manually recomposed for obtaining 2 cm and 4 cm thick breast tissues, and placed into cuboid-shaped PMMA sample holders. The remaining free airspace was filled with 4% formaldehyde solution. The full study was conducted in accordance with the Declaration of Helsinki and was approved by the local ethics committee. Written informed consent was gathered before enrolment within the study.

Histological workup

Representative tissue sections were dehydrated in an ascending alcohol series before embedding in hot paraffin wax. Since the sample size exceeded standard size, the procedure was performed manually by enwrapping the samples in a blotting paper and using non-standard slides ($7.5 \times 6.5\,\mathrm{cm}^2$). After solidification, the paraffin blocks were cut into 5 μm sections using a standard microtome and sections were stained with hematoxylin and eosin using standard protocols.

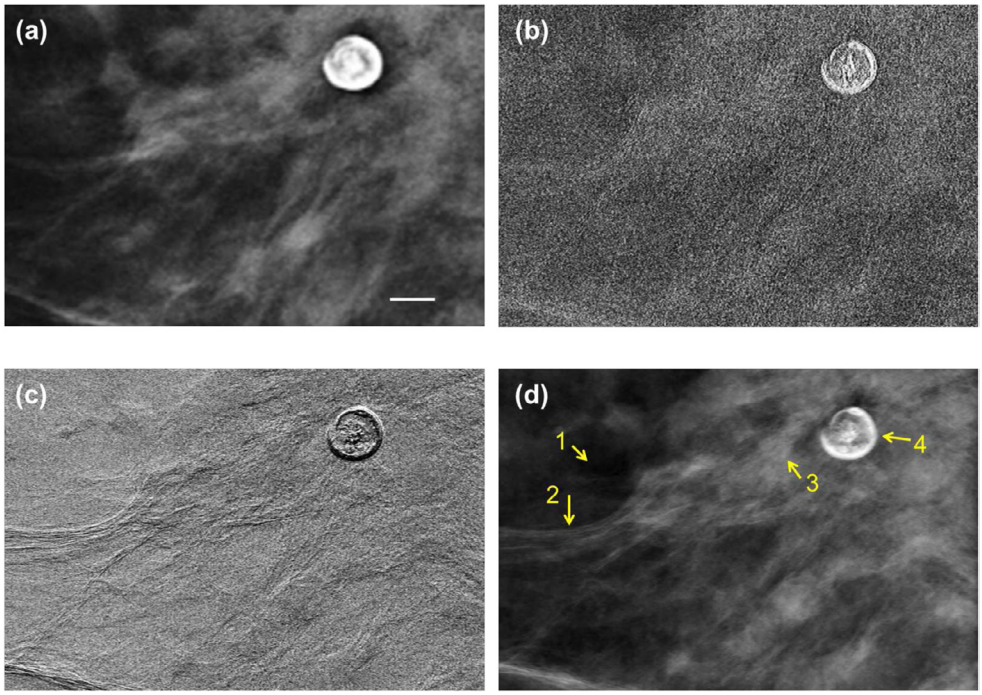

Figure 2. Conventional and XPCI images of a 2 cm thick breast sample, obtained from a mastectomy of a 61 year-old woman affected by an inflammatory carcinoma with lymphangitic carcinomatosis. (a) Conventional mammography acquired at 32 kVp (4.1 mGy MGD). Scale bar is 2 mm. (b)–(d) Synchrotron images acquired at 60 keV (0.12 mGy MGD): (b) attenuation image, (c) unprocessed EI-XPCI image, (d) retrieved phase image. The arrows in the retrieved phase image indicate various types of structures visible in the image: 1-fat tissue, 2-collagen strands, 3-glandular tissue, 4-macrocalcification.

Results

The first sample (thickness 2 cm, cross section $3 \times 3\,\text{cm}^2$) was obtained from a mastectomy of a 61 year-old woman affected by an inflammatory carcinoma with lymphangitic carcinomatosis. Images of this sample, obtained with the conventional mammography system operated at 32 kVp and with synchrotron radiation at 60 keV, are shown in figures 2(a)–(d), respectively. Due to the high x-ray energy employed, the synchrotron attenuation image (figure 2(b), MGD of 0.12 mGy) shows very limited contrast compared to the noise level, leading to negligible visualization of breast structures compared to the conventional image of figure 2(a) (MGD of 4.1 mGy). Conversely, despite having also been acquired at a low MGD of 0.12 mGy, the unprocessed -differential' EI-XPCI image (figure 2(c)) shows a good definition of collagen strands and glandular tissue, and of the internal structure of the macrocalcification. Image contrast is typical of 'differential' XPCI methods, showing only dark and bright fringes running along details' interfaces, where refraction of the beam occurs. As such, radiologists might find it suboptimal for diagnostic purposes. The typical 'area' contrast of mammography, however, is restored in the phase-retrieved image (figure 2(d), obtained by processing figure 2(c)), which gives breast structures an appearance similar to the conventional image, but arguably with better contrast-to-noise ratio and detail definition.

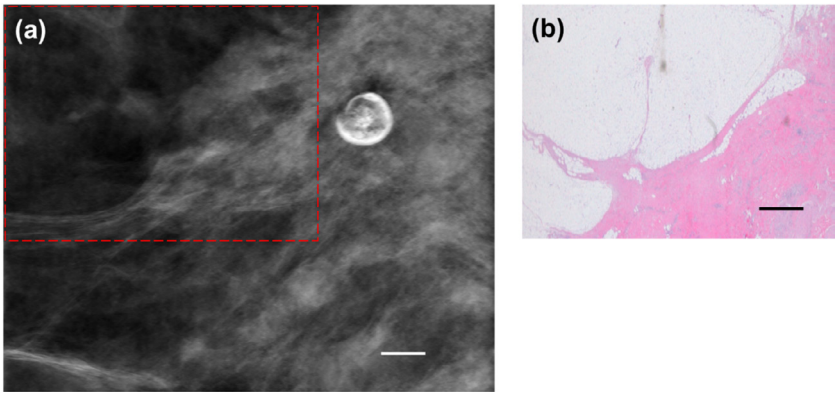

Figure 3. Comparison between retrieved XPCI phase image and histology. (a) Retrieved XPCI phase image of a 2 cm thick breast sample (0.12 mGy MGD). (b) Corresponding histological slice. Both scale bars are 2 mm. The histology shows a large region of fat tissue (white area), as well as a fibrous dysplasia of breast tissue (pink area) with small parts of glandular tissue within (violet area). In correlation with the histology, the XPCI image shows a sharp differentiation between fat tissue and the glandular/fibrous breast tissue, and the visualization of collagen strands within the fat tissue.

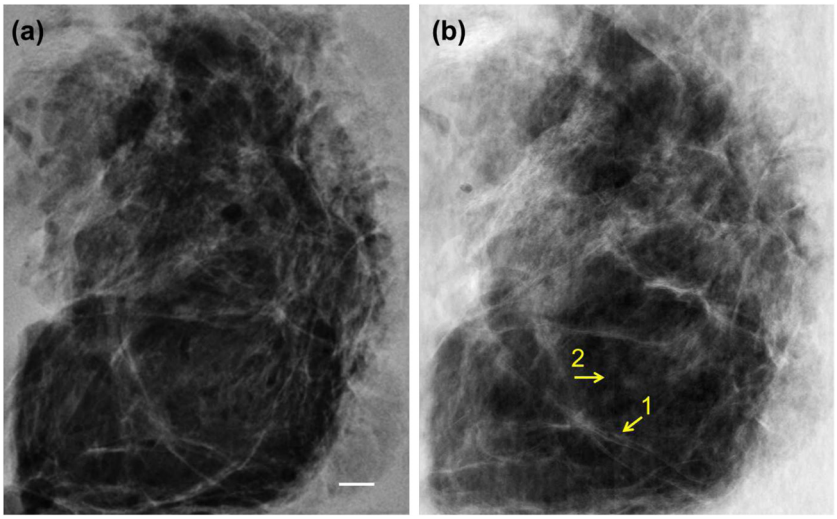

Figure 4. Conventional and XPCI images of a 4 cm thick breast sample, obtained from a mastectomy of a 58 year-old woman with a 6 cm invasive ductal carcinoma. Scale bar is 3 mm. (a) Conventional mammography acquired at 32 kVp (3.5 mGy MGD). (b) Retrieved phase image at 60 keV (0.12 mGy MGD). The arrows in image (b) indicate the main types of structures visible: 1-collagen strands, 2-fat tissue.

In order to further validate these results, histological workout was carried out after image acquisition. Comparison between the phase image and histology confirms the agreement between the structures visible in the two images (figure 3).

To confirm the potential of the method also for clinically relevant breast thicknesses, a thicker (4 cm, with a cross section of $5 \times 5\,\text{cm}^2$) sample was radiographed. This specimen was obtained from a mastectomy of a 58 year-old woman with a 6 cm invasive ductal carcinoma

(not present in the portion of the specimen made available for imaging). The conventional mammography and the synchrotron phase-retrieved image are presented in figures 4(a) and (b). The values of the MGDs were 3.5 mGy and 0.12 mGy, respectively. Despite the significant reduction in the delivered dose, all structures visible in the conventional image are also observable in the retrieved EI-XPCI image of figure 4(b), reflecting the situation observed with the thinner sample.

Discussion

While admittedly preliminary, these results demonstrate that the proposed method, based on combining high x-ray energy, a detector with ~100% efficiency at such energy, and a recently developed phase retrieval algorithm, can lead to very high dose reductions in mammography. It should be noted that the doses delivered with the conventional mammography setup in our experiment were larger than typical MGD values of 1–1.5 mGy used in clinical practice (Gennaro *et al* 2003). However, the sub-mGy doses reported in this article for XPCI still outperform typical clinical doses by about one order of magnitude. Moreover, only a small part of the obtained dose reductions can be attributed to the difference in efficiency between the detectors used in the XPCI and conventional setups. In fact, assuming a 60% detection efficiency for the Selenia Dimension system (Lazzari *et al* 2007) and a ~100% efficiency for the MAXIPIX detector, we can see that the different detectors can only account for a dose reduction of a factor ~1.67, compared to dose reductions of more than a factor 10 obtained in our XPCI experiment.

It is important to note that it is the interplay among the various factors listed above that enabled such a significant reduction. While the dose dependence on x-ray energy indicates the need for an increased energy value, this leads to the progressive disappearance of conventional attenuation-based contrast (figure 2(b)), as well as a decrease in the phase signal, albeit slower. This triggered the choice of the EI XPCI method, which was proven to lead to strong detectable signals also with weak phase perturbations at high x-ray energy (Diemoz *et al* 2013a). However, EI is a 'differential' XPCI method (Bravin *et al* 2013), and as such it leads to the collection of images which might be of difficult interpretation to a radiologist, as the conventional area contrast is replaced by a differential phase signal localized in narrow fringes running along tissue interfaces (figure 2(c)). This highlights the importance of appropriate image processing that can, through phase retrieval, provide images allowing easier readability. However, most phase retrieval algorithms require more than one input image (Bravin *et al* 2013), which is impractical from a clinical point of view and could also lead to higher radiation doses. To overcome this obstacle, a phase retrieval algorithm capable of providing high image quality while requiring only a single image as input was used (Diemoz *et al* 2015). Finally, a last hurdle is the reduced efficiency that most detectors have with increasing x-ray energy. This was overcome by the use of novel technology based on the hybridization of thick CdTe crystals to single photon counting readout chips. Not only does this type of detector guarantee near 100% efficiency, but it also leads to image noise minimization, thanks to its single-photon counting capabilities. This enables additional dose reduction, since it minimizes the number of detected photons needed to reach a given signal-to-noise level.

Future work will be dedicated to demonstrating improved lesion-glandular tissue contrast and tumour detectability, through the application of this XPCI method to a statistically significant number of samples representing different types of tumours, and to its implementation in table-top setups. Importantly, the transferability of the EI XPCI technique to compact laboratory setups has been proven in previous work (Olivo *et al* 2007a, 2013, Munro *et al* 2012,

Diemoz *et al* 2013b), also for high x-ray energies comparable to the ones used here (Ignatyev *et al* 2011, Olivo *et al* 2011). Previous work has also demonstrated the achromaticity (Diemoz *et al* 2013b, Endrizzi *et al* 2015) and resilience to broad spectra (Olivo *et al* 2007b, Ignatyev *et al* 2011) of the EI-XPCI approach which, together with the quoted effectiveness at high energy, leaves ample margins for optimization of a hard x-ray spectrum produced by e.g. a tungsten rotating source through an appropriate choice of filters.

Mammography was selected because of the radiosensitive nature of the breast (ICRP 2007), which makes achieving dose reductions extremely important. Moreover, there is significant on-going debate on the benefits and drawbacks of screening campaigns, the latter mostly related to the risk of inducing secondary cancers through exposure of the breast to radiation (O'Connor *et al* 2010, De Gelder *et al* 2011, Yaffe *et al* 2011). In this context, being able to substantially reduce this exposure would significantly change the boundary conditions, arguably shifting the balance towards the benefits. Moreover, the introduction of significant dose reduction strategies in mammography could trigger research in the same direction in other areas of diagnostic radiology. Although technically more challenging, it would be extremely important in the longer term to achieve dose reductions in computed tomography (CT). Indeed, despite accounting for a small percentage in terms of total number of x-ray related procedures, CT contributes to a substantial fraction of the total radiation dose to the population due to medical examinations (NCRP 2009, Smith-Bindman *et al* 2009). The combination of strategies similar to the ones described above with e.g. new CT algorithms capable of reconstructing the 3D structure of the object with few projections (Zhao *et al* 2012) could offer opportunities in this sense.

Acknowledgments

H Requardt, T Brochard and C Nemoz from ID17 beamline at the ESRF are kindly acknowledged for the support given in the realization of the experiment. This work is funded by the UK Engineering and Physical Sciences Research Council (EPSRC, grant EP/I021884/1) and by the German DFG-Cluster of Excellence Munich-Centre for Advanced Photonics (EXE158). P C Diemoz is partly funded by a Marie Curie Career Integration Grant (No. PCIG12-GA-2012-333990) within the Seventh Framework Programme of the European Union. The high-energy version of the detector used in this study was developed within the CALIPSO European project from the Seventh Framework program of the European Union (Grant No. 312284). The ESRF is acknowledged for the provision of beamtime and computational resources.

References

Boone J M 1999 Glandular breast dose for monoenergetic and high-energy x-ray beams: Monte Carlo assessment *Radiology* **213** 23–37

Bravin A, Coan P and Suortti P 2013 X-ray phase-contrast imaging: from pre-clinical applications towards clinics *Phys. Med. Biol.* **58** R1–35

Castelli E *et al* 2011 Mammography with synchrotron radiation: first clinical experience with phase-detection technique *Radiology* **259** 684–94

Davis T J, Gao D, Gureyev T E, Stevenson A W and Wilkins S W 1995 Phase-contrast imaging of weakly absorbing materials using hard x-rays *Nature* **373** 595–8

De Gelder R, Draisma G, Heijnsdijk E A M and De Koning H J 2011 Population-based mammography screening below age 50: balancing radiation-induced versus prevented breast cancer deaths *Br. J. Cancer* **104** 1214–20

Deutsches Institut für Normung (DIN) 2013 Report 6868—image quality assurance in diagnostic x-ray departments, part 162: RöV acceptance test of x-ray installations for digital mammography (www.din.de/en/getting-involved/standards-committees/nar/standards/wdc-beuth:din21:178453704)

Diemoz P C, Endrizzi M, Zapata C E, Pešić Z D, Rau C, Bravin A, Robinson I K and Olivo A 2013a X-ray phase-contrast imaging with nanoradian angular resolution *Phys. Rev. Lett.* **110** 138105

Diemoz P C, Hagen C K, Endrizzi M and Olivo A 2013b Sensitivity of laboratory based implementations of edge illumination x-ray phase-contrast imaging *Appl. Phys. Lett.* **103** 244104

Diemoz P C, Vittoria F A, Hagen C K, Endrizzi M, Coan P, Bravin A, Wagner U H, Rau C, Robinson I K and Olivo A 2016 A single-image retrieval method for edge illumination x-ray phase-contrast imaging: application and noise analysis *Phys. Medica* at press (doi: 10.1016/j.ejmp.2016.07.093)

Diemoz P C *et al* 2015 Single-image phase retrieval using an edge illumination x-ray phase-contrast imaging setup *J. Synchrotron Radiat.* **22** 1072–7

Endrizzi M, Vittoria F A, Kallon G, Basta D, Diemoz P C, Vincenzi A, Delogu P, Bellazzini R and Olivo A 2015 Achromatic approach to phase-based multi-modal imaging with conventional x-ray sources *Opt. Express* **23** 16473–80

Gennaro G, Baldelli P, Taibi A, Di Maggio C and Gambaccini M 2003 Patient dose in full-field digital mammography: an Italian survey *Eur. Radiol.* **14** 645–52

Grandl S, Willner M, Herzen J, Mayr D, Auweter S D, Hipp A, Pfeiffer F, Reiser M and Hellerhoff K 2013 Evaluation of phase-contrast CT of breast tissue at conventional x-ray sources—presentation of selected findings *Z. Med. Phys.* **23** 212–21

Hagen C K, Munro P R T, Endrizzi M, Diemoz P C and Olivo A 2014 Low-dose phase contrast tomography with conventional x-ray sources *Med. Phys.* **41** 070701

Hammerstein G R, Miller D W, White D R, Masterson M E, Woodard H Q and Laughlin J S 1979 Absorbed radiation dose in mammography *Radiology* **130** 485–91

Henke B, Gullikson E and Davis J 1993 X-ray interactions: photoabsorption, scattering, transmission and reflection at $E = 50$–$30\,000$ eV, $Z = 1$–92 *At. Data Nucl. Data Tables* **54** 181–342

ICRP 2007 *The 2007 Recommendations of the International Commission on Radiological Protection* (*Annals of the ICRP, ICRP publication 103* vol 37) (Oxford: Elsevier)

Ignatyev K, Munro P R T, Chana D, Speller R D and Olivo A 2011 Coded apertures allow high-energy x-ray phase contrast imaging with laboratory sources *J. Appl. Phys.* **110** 014906

Keyriläinen J *et al* 2008 Toward high-contrast breast CT at low radiation dose *Radiology* **249** 321–7

Lazzari B, Belli G, Gori C and Rosselli Del Turco M 2007 Physical characteristics of five clinical systems for digital mammography *Med. Phys.* **34** 2730–43

Mittone A, Bravin A and Coan P 2014 Radiation dose in breast CT imaging with monochromatic x-rays: simulation study of the influence of energy, composition and thickness *Phys. Med. Biol.* **59** 2199–217

Mittone A *et al* 2013 An efficient numerical tool for dose deposition prediction applied to synchrotron medical imaging and radiation therapy *J. Synchrotron Radiat.* **20** 785–92

Munro P R T, Ignatyev K, Speller R D and Olivo A 2012 Phase and absorption retrieval using incoherent x-ray sources *Proc. Natl Acad. Sci. USA* **109** 13922–7

National Council on Radiation Protection and Measurements 2009 *Ionizing Radiation Exposure of the Population of the United States* (*NCRP Report* vol 160) (Bethesda, MD: NCRP)

O'Connor M K, Li H, Rhodes D J, Hruska C B, Clancy C B and Vetter R J 2010 Comparison of radiation exposure and associated radiation-induced cancer risks from mammography and molecular imaging of the breast *Med. Phys.* **37** 6187

Olivo A, Ignatyev K, Munro P R T and Speller R D 2011 Noninterferometric phase-contrast images obtained with incoherent x-ray sources *Appl. Opt.* **50** 1765–9

Olivo A and Speller R D 2007a A coded-aperture technique allowing x-ray phase contrast imaging with conventional sources *Appl. Phys. Lett.* **91** 074106

Olivo A and Speller R D 2007b Modelling of a novel x-ray phase contrast imaging technique based on coded apertures *Phys. Med. Biol.* **52** 6555–73

Olivo A *et al* 2001 An innovative digital imaging set-up allowing a low-dose approach to phase contrast applications in the medical field *Med. Phys.* **28** 1610–9

Olivo A *et al* 2013 Low-dose phase contrast mammography with conventional x-ray sources *Med. Phys.* **40** 090701

Pfeiffer F, Weitkamp T, Bunk O and David C 2006 Phase retrieval and differential phase-contrast imaging with low-brilliance x-ray sources *Nat. Phys.* **2** 258–61

Ponchut C, Rigal J M, Clément J, Papillon E, Homs A and Petitdemange S 2011 MAXIPIX, a fast readout photon-counting x-ray area detector for synchrotron applications *J. Instrum.* **6** C01069

Ruat M and Ponchut C 2012 Characterization of a pixelated CdTe x-ray detector using the Timepix photon-counting readout chip *IEEE Trans. Nucl. Sci.* **59** 2392–401

Smith-Bindman R, Lipson J, Marcus R, Kim K P, Mahesh M, Gould R, Berrington de Gonzalez A and Miglioretti D L 2009 Radiation dose associated with common computed tomography examinations and the associated lifetime attributable risk of cancer *Arch. Intern. Med.* **169** 2078–86

Snigirev A, Snigireva I, Kohn V, Kuznetsov S and Schelokov I 1995 On the possibilities of x-ray phase contrast microimaging by coherent high-energy synchrotron radiation *Rev. Sci. Instrum.* **66** 5486–92

Stampanoni M, Wang Z, Thüring T, David C, Roessl E, Trippel M, Kubik-Huch R A, Singer G, Hohl M K and Hauser N 2011 The first analysis and clinical evaluation of native breast tissue using differential phase-contrast mammography *Invest. Radiol.* **46** 801–6

Sztrokay A *et al* 2013 Assessment of grating-based x-ray phase-contrast CT for differentiation of invasive ductal carcinoma and ductal carcinoma *in situ* in an experimental *ex vivo* set-up *Eur. Radiol.* **23** 381–7

Wilkins S W, Nesterets Y I, Gureyev T E, Mayo S C, Pogany A and Stevenson A W 2014 On the evolution and relative merits of hard x-ray phase-contrast imaging methods *Phil. Trans. R. Soc.* A **372** 20130021

Yaffe M J and Mainprize J G 2011 Risk of radiation-induced breast cancer from mammographic screening *Radiology* **258** 98–105

Zhao Y *et al* 2012 High-resolution, low-dose phase contrast x-ray tomography for 3D diagnosis of human breast cancers *Proc. Natl Acad. Sci. USA* **109** 18290–4